Hindawi
Advances in Materials Science and Engineering
Volume 2021, Article ID 6428018, 11 pages
https://doi.org/10.1155/2021/6428018

Research Article

Experimental Study on the High-Temperature Shear Performance of Asphalt Mixtures

Jia'ning Huang,[1] Ruiduo Li ,[2] Song Yin,[1] and Pengfei Liu[1]

[1]*School of Civil Engineering and Architecture, Zhongyuan University of Technology, Zhengzhou, Henan 450007, China*
[2]*School of Civil and Transportation Engineering, Henan University of Urban Construction, Pingdingshan, Henan 467036, China*

Correspondence should be addressed to Ruiduo Li; lird2010@126.com

Received 9 April 2021; Revised 11 August 2021; Accepted 30 August 2021; Published 9 September 2021

Academic Editor: Robert Černý

The influence of temperature on the shear performance of asphalt mixtures and the feasibility of using the deformation strength as an index of the high-temperature shear performance of these mixtures were explored in this study. Taking AC-13C and AC-20C asphalt mixtures as the research objects, uniaxial compression, rutting, deformation strength, and uniaxial static load creep tests were carried out at temperatures 40°C, 45°C, 50°C, 55°C, and 60°C. The correlations between the deformation strength and modulus of resilience, compressive strength, dynamic stability, and stiffness of the asphalt mixtures were studied. The test results show that the influence of temperature on the compressive strength, resilience modulus, and deformation strength of the asphalt mixtures decreases significantly as the temperature increased, and the rutting deformation of the two kinds of asphalt mixtures increased as the temperature increased. Strong correlations exist between the deformation strength and the modulus of resilience, the compressive strength, and the dynamic stability of asphalt mixtures, so the deformation strength can be used as an evaluation index of the high-temperature shear performance of asphalt mixtures.

1. Introduction

Asphalt pavement diseases mainly include cracks, ruts, and pits. The rut disease also includes fluid ruts and structural ruts. The former refers to the repeated action of wheel rolling under high-temperature conditions when the load stress exceeds the stability limit of the asphalt mixture. The latter refers to the permanent deformation of each structural layer under the asphalt surface, including the roadbed, due to the load exceeding the strength of the pavement layer. The rutting of asphalt pavement is mainly related to the permanent deformation of asphalt mixtures at high temperatures. Therefore, it is essential to reduce the rutting rate of asphalt pavement by studying the permanent deformation characteristics of asphalt mixtures at high temperatures.

At present, creep tests are mainly used to study the high-temperature permanent deformation characteristics of asphalt mixtures [1]. Through creep tests, the constitutive relationship of asphalt mixtures under loading can be obtained, and then leaching can reflect the stress state and deformation behavior of green mixtures.

Molenaar et al. [2] and Hafez [3] studied the performance of asphalt mixtures through unconfined creep tests. Jiang et al. [4] examined the permanent deformation characteristics of asphalt mixtures under multiple repeated loads. Moriyoshi et al. [5] investigated the strain distribution law inside asphalt mixtures at high temperatures through rutting tests. Karami et al. [6] analyzed the permanent deformation of asphalt pavement mixtures through dynamic creep tests.

The uniaxial static penetration test method has been extensively used to study the high-temperature permanent deformation characteristics of asphalt mixtures due to its advantages of simple instrumentation and convenient operation [7, 8]. Golsefidi and Sahaf [9] studied the influence of different loading methods on the shear performance of asphalt mixtures. Lijun et al. [10–12] proposed the use of a uniaxial penetration test to evaluate the shear performance of asphalt mixtures and further used a uniaxial penetration

repeated shear test to study the permanent deformation characteristics of asphalt mixtures under different stress levels [13, 14]. The principle of the uniaxial penetration test is the application of a load at a loading rate of 1 mm/min on a cylindrical specimen to simulate the wheel load on the actual road surface, as shown in Figure 1(a). The test specimen is a cylinder with dimensions of $\Phi 100\,\text{mm} \times 100\,\text{mm}$ or $\Phi 150\,\text{mm} \times 100\,\text{mm}$. The round, flat steel indenters have a diameter of 28.5 mm or 42.0 mm (Figure 1(b)). Huang et al. [15] obtained the corresponding test parameters through numerical simulation of the uniaxial penetration creep test of a rutting board by using the finite element method. Then, the rutting deformation of flexible base asphalt pavement was estimated and analyzed by using the finite element method. Cai [16] identified a linear relationship between the shear strength and the temperature by using a uniaxial penetration test of asphalt mixtures at different temperatures.

The above research results demonstrate that the uniaxial penetration test can better simulate the actual pavement stress state under wheel loading. However, this test also has some defects. The loading rate of the uniaxial penetration test is 1 mm/min, which can be approximately simplified to a static load. This situation is quite different from the dynamic load action of wheels running at high speed. Thus, the stress distribution of an asphalt mixture specimen is very different from that of the actual asphalt pavement. Second, the uniaxial static load creep test is advantageous because it uses simple equipment and is convenient and practical. However, in uniaxial static load creep tests under the condition of high-temperature, the sample will undergo accelerated creep and damage occurs. Third, the uniaxial static load creep test cannot reflect the lateral restraint of asphalt mixtures under vehicle loads. Finally, in a uniaxial penetration test, cylindrical steel indenters with flat bottoms cause stress concentrations in asphalt mixtures at the indenter edges.

Based on the aforementioned research, a cylindrical uniaxial compression test and a rutting test were carried out for AC-13C and AC-20C asphalt mixtures. The pressure head of the single-axle static load penetration test was improved to more closely simulate the load action form of vehicle tires on asphalt pavement. Then, the deformation strength test and the uniaxial penetration creep test were carried out with the improved circular indenter. The correlations between the deformation strength and the compressive rebound modulus, the compressive strength, and the dynamic stability of asphalt mixtures were studied. The feasibility of using the deformation strength as an evaluation index of the high-temperature shear performance of asphalt mixtures was discussed.

2. Test Materials

2.1. Preparation of Asphalt Mortar

2.1.1. Asphalt. The asphalt was No. 70 grade A road petroleum asphalt. The basic physical properties of asphalt were determined according to "Test Methods of Bitumen and Bituminous Mixtures for Highway Engineering" (JTG E20–2011) [17] standard test methods. The results are shown in Table 1.

2.1.2. Physical Properties of Aggregates. The mineral materials used in the test were coarse aggregates (limestone, from Jiaxian, Henan, China), fine aggregates (sand and detritus, sand from LuShan, Henan, China; detritus is the lower part of the 2.36 mm sieve when the quarry breaks the stone), and ore powder. The coarse aggregates included the following three grades: 5–10 mm, 10–15 mm, and 15–20 mm. The fine aggregates included sand and gravel. According to the "Test Methods of Aggregate for Highway Engineering" (JTG E42-2005) [18], the net basket method was used to measure the relative density of the gross volume of the coarse aggregate. The apparent relative density and the gross relative density of the fine aggregates were measured using the volumetric flask method and the slump cylinder method. The performance indices of the coarse aggregate and fine aggregates obtained through the tests are listed in Tables 2 and 3.

2.2. Preparation of Asphalt Mixture Specimens. According to the median gradation of AC-13C and AC-20C asphalt mixtures specified in "Technical specifications for construction of highway asphalt pavements" (JTG F40-2004) [19], the mineral aggregate gradation composition is designed, which can ensure the stability of the mineral aggregate gradation of the specimen and reduce the test error caused by the heterogeneity of raw materials. Mineral gradation composition of AC-13C and AC-20C asphalt mixtures according to the median gradation composition of asphalt mixtures designed for crude dense-gradation asphalt mixture is shown in Table 4.

According to the Marshall test, the optimal asphalt contents of the AC-13C and AC-20C asphalt mixtures are 4.76% and 4.03%, respectively. The preparation of the raw minerals and bitumen was in accordance with the requirements of the "Test Methods of Bitumen and Bituminous Mixtures for Highway Engineering" (JTG E20–2011) [17] and the "Test Methods of Aggregate for Highway Engineering" (JTG E42–2005) [18]. Figure 2 shows the preparation of the cylindrical specimens with diameters and heights of 100 mm by static pressing molding.

3. Test Experiment

3.1. Test of Uniaxial Compression. Figure 3 shows the electronic universal testing machine, which can automatically load and unload, collect data, and generate displacement curves and other curves for test specimens. The completed AC-13C and AC-20C specimens were subjected to uniaxial compression tests at 40°C, 45°C, 50°C, 55°C, and 60°C using the electronic universal testing machine. The compressive strength and compressive rebound modulus of both specimens were obtained.

3.2. Rutting Test. Figure 4 shows the rut specimen with length × width × height dimensions of 300 mm ×

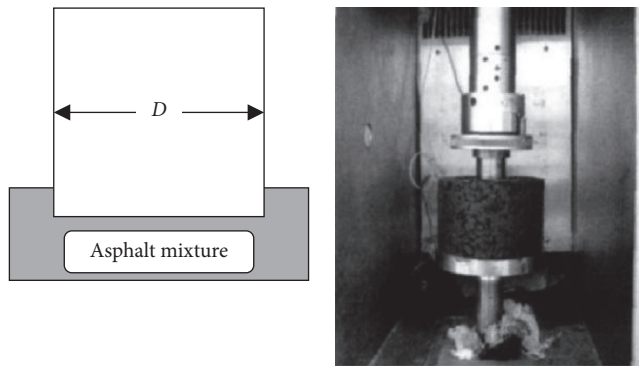

(a) (b)

Figure 1: Single-axis penetration test device. (a) Diagram of the uniaxial penetration test head. (b) Uniaxial penetration test.

Table 1: Basic technical characteristics of asphalt.

Project		Unit	Measured value
Penetration (100 g, 5 s)	5°C	0.1 mm	6.7
	15°C	0.1 mm	17.9
	25°C	0.1 mm	60.6
PI		—	−1.04
Equivalent softening point (T800)		°C	49.7
Equivalent breaking point	T1. 2	°C	−10.4
Ductility	5°C	cm	1.4
	15°C	cm	35.6
Softening point		°C	48.3

300 mm × 5 mm made in accordance with "Test Methods of Bitumen and Bituminous Mixtures for Highway Engineering" (JTG E20–2011) [17].

Figure 5 shows the rutting test instrument produced by Italian Controls and a photo of an experiment with it.

The dynamic stability of the AC-13C and AC-20C asphalt mixtures was calculated according to the following equation:

$$\mathrm{DS} = \frac{(t_1 - t_2) \times N}{d_2 - d_1} \times C_1 \times C_2. \quad (1)$$

In this equation, DS is the dynamic stability of the asphalt mixture (times/mm), d_1 is the deformation corresponding to time t_1 (mm), d_2 is the deformation corresponding to time t_2 (mm), C_1 is the type coefficient of the test instrument (1.0), C_2 is the specimen coefficient, and N is the test rolling frequency, which is usually 42 times/min. The width of the specimen was 300 mm.

3.3. Test of Deformation Strength. Figure 6 shows a schematic diagram of the rutting damage caused by vehicles on asphalt pavement. The research shows that the shear performance of an asphalt mixture is one of the most important factors affecting the rutting of the asphalt pavement. Figure 7 presents how Doh et al. [20] adopted the deformation strength method (SD method) to simulate a vehicle load. In the test process, the loading rate of 50.8 mm/min better simulates the vibration load generated by tires when a vehicle is running at high speeds.

Based on the uniaxial penetration test, the bottom of the original indenter was rounded by the SD method. Therefore, the indenter was more similar to the load action mode of an actual vehicle tire on a road surface. Figure 8 shows an illustration of the improved indenter. At the beginning of the loading stage, the asphalt specimen was consolidated and then allowed to sag. Figure 9 shows the specimen with cracks appearing and expanding until failure caused by continuous loading.

The deformation strength calculated by the SD method is influenced by both the shear strength and the plastic deformation (see equation (2) for the deformation strength calculation formula of the SD method). Compared with the uniaxial penetration test based on elastic mechanics, this method can better simulate the real situation of the asphalt pavement under a vehicle load,

$$S_D = \frac{4P}{\pi\left[D - 2\left(r - \sqrt{2ry - y^2}\right)\right]^2}. \quad (2)$$

In this equation, S_D is the deformation strength (MPa), P is the largest load (N), D is the diameter of the indenter (mm), r is the indenter bottom arc radius (Figure 8) (mm), and y is the maximum vertical deformation that occurs when the specimen is damaged (mm).

The electronic universal testing machine shown in Figure 3 was employed for the loading test (with the improved indenter). The test loading rate was 50.8 mm/min. The pressure of the specimen failure was taken as the maximum load. Formula (2) was applied to compute the deformation strength of the asphalt mixture. Three parallel tests were performed for each sample, and the average value was taken as the result.

3.4. Test of Uniaxial Penetration Creep. The improved uniaxial penetration creep test can avoid the stress concentration around the pressure head caused by the traditional penetration test and better reflect the vehicle tire load form. Therefore, the penetration head used for the deformation strength test mentioned above was used in the uniaxial

Table 2: Performance indices of the coarse aggregates.

Nominal diameter (mm)	Los Angeles attrition loss (%)	Apparent relative density (t/m^3)	Water absorption (%)	Needle-flake particle content (%)
5–10	21.2	2.77	1.50	18.9
10–15	17.3	2.86	0.43	11.3
10–20	14.8	2.84	0.45	12.5

Table 3: Performance indices of the fine aggregates.

Name	Apparent relative density (t/m^3)	Silt content (%)
Sand	2.65	4.4

Table 4: Mineral aggregate gradation ranges of the AC-13 and AC-20C asphalt mixtures.

AC-13C				AC-20C			
Screen-aperture (mm)	Upper limit (%)	Lower limit (%)	Midvalue (%)	Screen-aperture (mm)	Upper limit (%)	Lower limit (%)	Midvalue (%)
—	—	—	—	26.5	100	100	100
—	—	—	—	19	100	90	95
16	100	100	100	16	92	78	85
13.2	100	90	95	13.2	80	62	71
9.5	85	68	76.5	9.5	72	50	61
4.75	68	38	53	4.75	56	26	41
2.36	50	24	37	2.36	44	16	30
1.18	38	15	26.5	1.18	33	12	22.5
0.6	28	10	19	0.6	24	8	16
0.3	20	7	13.5	0.3	17	5	11
0.15	15	5	10	0.15	13	4	8.5
0.075	8	4	6	0.075	7	3	5

(a) (b)

Figure 2: Sample making. (a) Molds used for testing the molded specimens. (b) Molded parts of the specimens.

penetration creep test for asphalt mixtures in this study. The test temperatures were 40°C, 45°C, 50°C, 55°C, and 60°C, and the pressure was 220 N.

4. Interpretations of the Experimental Results

4.1. Relationships between the Compressive Strength, the Compressive Resilience Modulus, and the Temperature of the Asphalt Mixtures. Figure 10 is the correlation analysis diagram of the compressive strength and the temperature of the AC-13C and AC-20C asphalt mixtures. As the temperature increased, the compressive strength of the two asphalt mixtures decreased gradually. At 40°C, the compressive strength of the AC-13C asphalt mixture was greater than that of the AC-20C mixture. As the temperature increased, this advantage gradually disappeared and became a disadvantage. When the temperature increased to 60°C, the compressive strength of the AC-13C asphalt mixture was slightly lower than that of the AC-20C mixture. As the temperature increased from 40°C to 60°C, the compressive strength of the AC-13C asphalt mixture decreased by 51.82% and that of the AC-20C asphalt mixture decreased by 43.83%. The compressive strength of the AC-13C asphalt mixture was greatly affected by the temperature increase. Moreover, the compressive strength of the AC-13C and AC-20C asphalt mixtures exhibits a linear exponential decrease as the temperature increased, and the coefficients of determination of the two asphalt mixtures were 0.9587 and 0.9630, respectively. Interestingly, in the case of very high temperature (60°C), two asphalt mixtures were observed to possess a strength that was lower than the predicted value of the exponential curve. Because, at this temperature, the

Figure 3: CMT5105 microcomputer-controlled electronic universal testing machine.

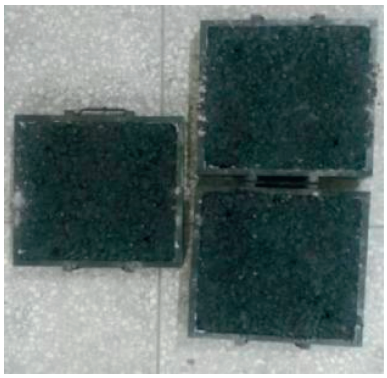

Figure 4: Rut specimen.

Figure 5: Rut tester.

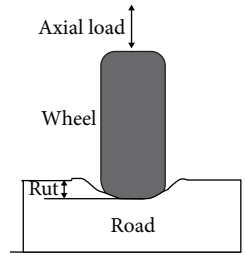

Figure 6: Schematic diagram of rutting disease.

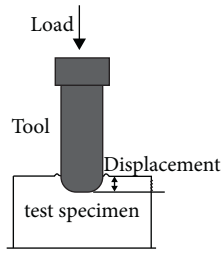

Figure 7: Schematic diagram of the SD method.

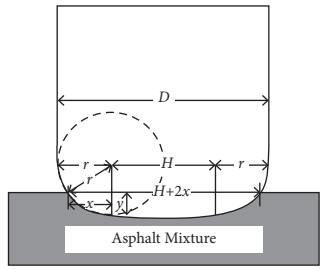

Figure 8: Improved indenter ($D = 40$ mm, $r = 10$ mm).

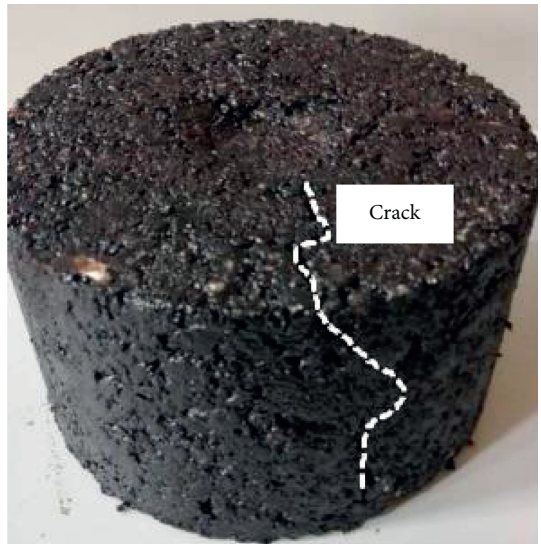

Figure 9: Failure mode of the failure specimen (AC-13C).

contribution of the cohesion between the aggregates to the strength was almost zero, and the strength of the asphalt mixture was probably completely provided by the strength of the aggregate itself and the friction between the aggregates.

Figure 11 presents the correlation analysis diagram of the compressive resilience modulus and the temperature of the asphalt mixture. As the temperature increased, the compressive resilience modulus of the two asphalt mixtures decreased gradually. The compressive resilience modulus of the AC-13C asphalt mixture was lower than that of the AC-20C mixture. As the temperature increased to 60°C, the compressive strength of the AC-13C asphalt mixture

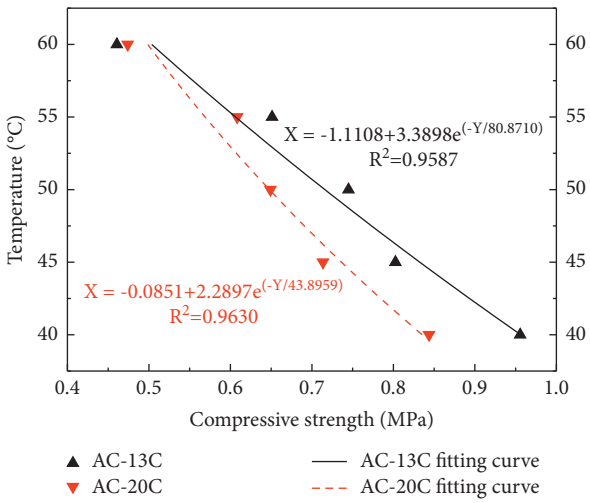

Figure 10: Correlation analysis of the compressive strength and the temperature of the AC-13C and AC-20C asphalt mixtures.

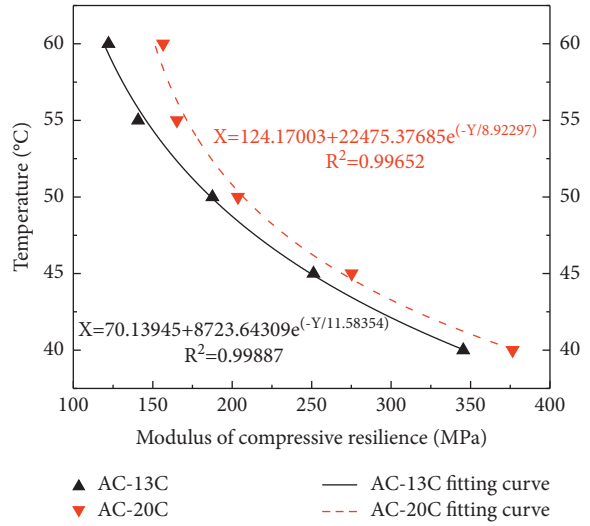

Figure 11: Correlation analysis between the compressive resilience modulus and the temperature of the AC-13C and AC-20C asphalt mixtures.

decreased by 64.64%, and that of the AC-20C asphalt mixture decreased by 58.42%. The compressive resilience modulus of the two asphalt mixtures exhibited a linear exponential decrease as the temperature increased, and the determination coefficients were 0.99887 and 0.99652, respectively.

4.2. Relationships between the Rutting Deformation, Dynamic Stability, and Temperature of the Asphalt Mixtures. Figures 12 and 13 show the logarithmic correlation analysis diagrams of the rutting deformation and time for the AC-13C and AC-20C asphalt mixtures, respectively. The rutting deformation of the two asphalt mixtures increased gradually with time. Simultaneously, the higher the temperature was, the greater the rutting deformation of the two asphalt mixtures was. The final rutting deformation of the AC-13C

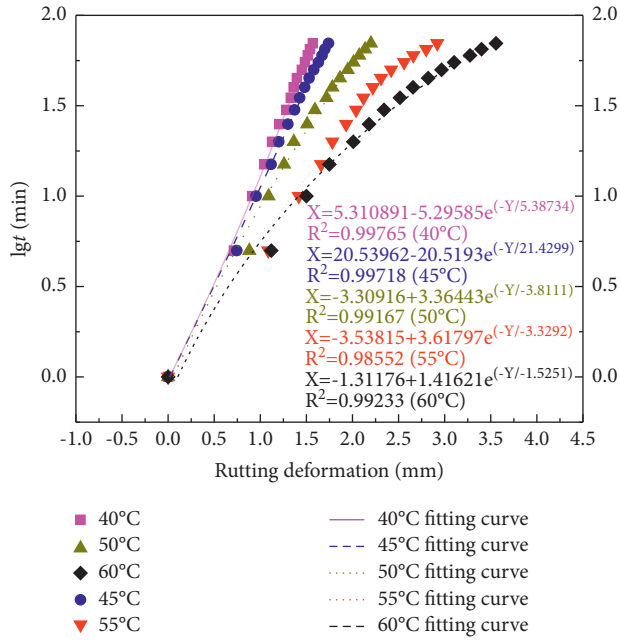

Figure 12: Correlation analysis of the AC-13C asphalt mixtures rutting deformation and the logarithm of time.

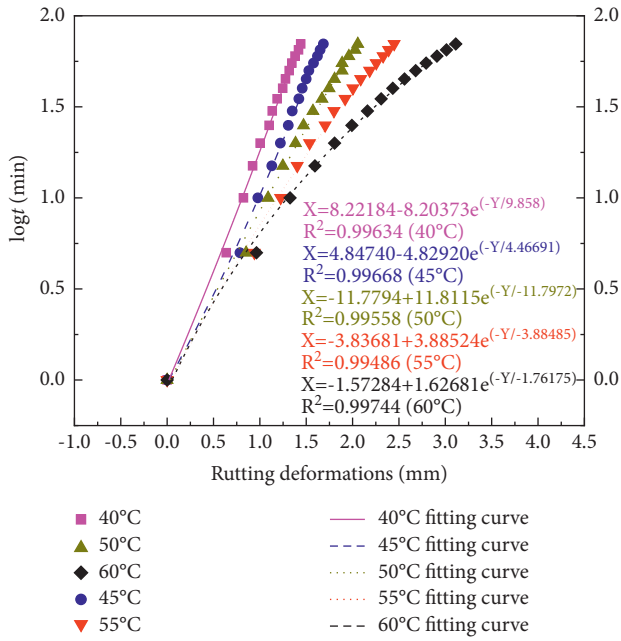

Figure 13: Correlation analysis of the AC-20C asphalt mixtures rutting deformation and the logarithm of time.

asphalt mixture at 60°C was 2.264 times that at 40°C, and that of the AC-20C mixture at 60°C was 2.160 times that at 40°C. Therefore, the temperature has a great influence on the rutting deformation of the asphalt mixtures. The rutting deformation of the two asphalt mixtures showed a first-order linear exponential growth relationship with the logarithm of time.

Figure 14 exhibits the correlation analysis diagram of the dynamic stability and temperature of the two asphalt

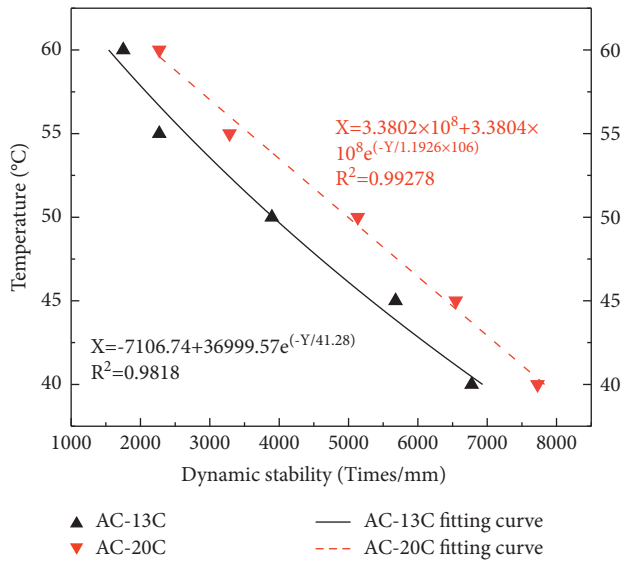

Figure 14: Correlation analysis of the dynamic stability and temperature of the AC-13C and AC-20C asphalt mixtures.

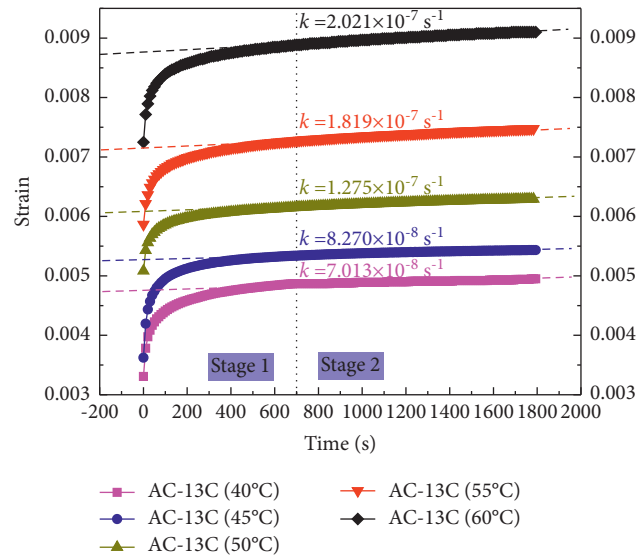

Figure 15: Creep curve of the AC-13C asphalt mixture at different temperatures.

mixtures. As the temperature increased, the dynamic stability of the two asphalt mixtures decreased gradually. The dynamic stability of the AC-13C asphalt mixture was lower than that of the AC-20C mixture. When the temperature increased from 40°C to 60°C, the compressive strength of the AC-13C asphalt mixture decreased by 74.14% and that of the AC-20C asphalt mixture decreased by 70.61%. The dynamic stability of the two asphalt mixtures exhibited a first-order linear exponential decrease as the temperature increased. The determinative coefficients of the two asphalt mixtures were 0.98180 and 0.99278.

4.3. Relationship between the Uniaxial Penetration Creep of the Asphalt Mixtures and Temperature. It can be seen from the data in Figures 15 and 16 that the creep curve of asphalt mixtures can be divided into two stages: at Stage 1, the creep rates decreased with time, and at Stage 2, the creep tends to be steady, the steady creep rates to be constant, and the creep curves were similar to straight lines. The creep rates of the two asphalt mixtures at different temperatures are presented in Figures 15 and 16. It can be seen from the figures that the transient strains of AC-13C and AC-20C asphalt mixtures increase as the test temperature increased, and at the same time, the higher the temperature, the greater the creep. At the same temperature, the transient strain of the AC-20C asphalt mixture was smaller than that of the AC-13C asphalt mixture. In stage 2, the creep rates of both asphalt mixtures increase as the temperature increased; however, at the same temperature, the creep rate of the AC-13C asphalt mixture was smaller than that of the AC-20C asphalt mixture.

The stiffness modulus parameters were extracted from the creep curves, and Figure 17 presents the variation in the stiffness modulus with temperature. As the temperature increased, the stiffness modulus of the two asphalt mixtures decreased gradually, signifying that as the temperature increased, the cementitious material in the asphalt mixture

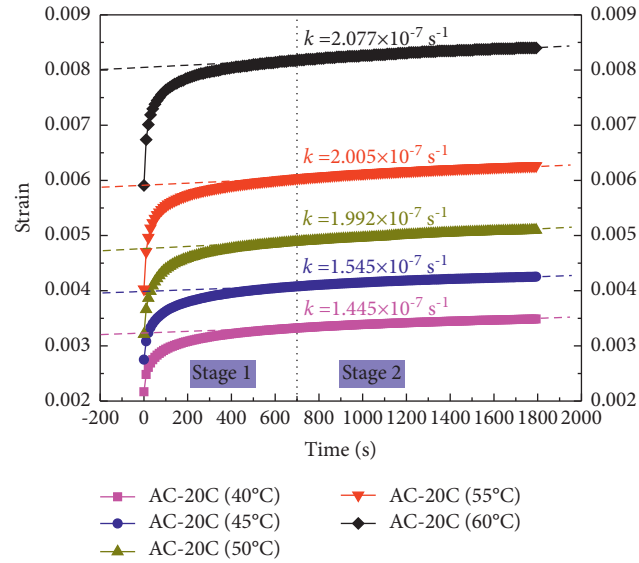

Figure 16: Creep curve of the AC-20C asphalt mixture at different temperatures.

softened, and the friction between aggregates decreased, thus reducing the deformation resistance of the asphalt mixture. The stiffness modulus of the asphalt mixture showed a good regularity with the temperature. The determination coefficients of the AC-13C and AC-20C mixtures were 0.9961 and 0.9985, respectively.

4.4. Correlation Analysis of the Deformation Strength, Compressive Strength, Compressive Resilience Modulus, and Dynamic Stability of the Asphalt Mixtures. Figure 18 shows the correlation analysis diagram between the deformation strength and temperature of the AC-13C and AC-20C asphalt mixtures. As the temperature increased, the

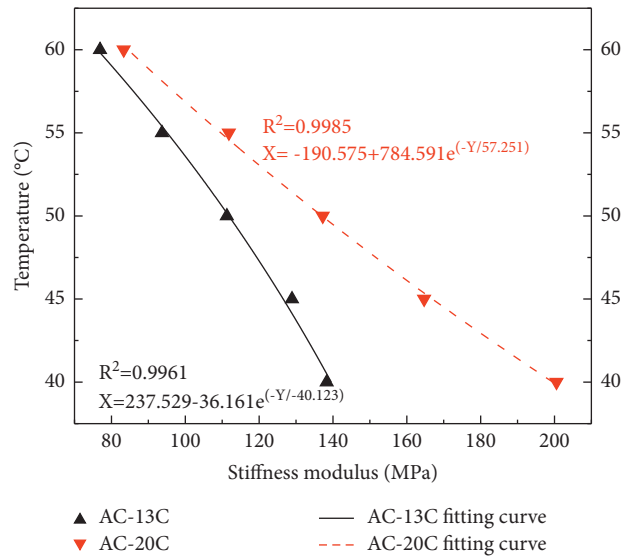

Figure 17: Correlation analysis diagram of the stiffness modulus and the temperature of the AC-13C and AC-20C asphalt mixtures.

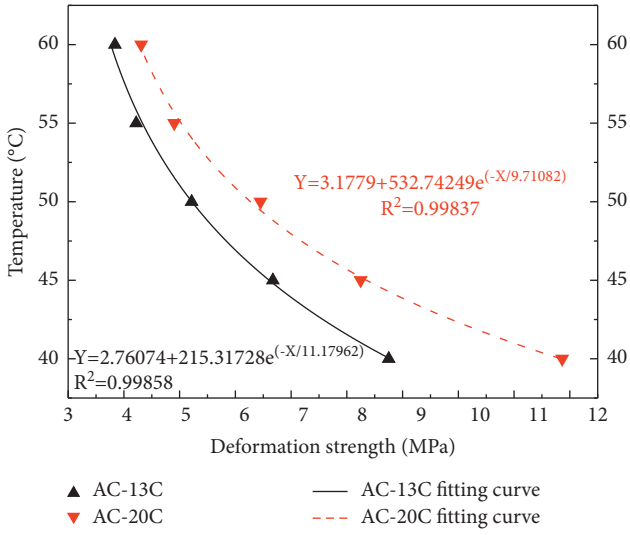

Figure 18: Correlation analysis of the deformation strength and temperature of the AC-13C and AC-20C asphalt mixtures.

deformation strength of both asphalt mixtures decreased gradually. At the same temperature, the deformation strength of the AC-13C asphalt mixture was lower than that of the AC-20C mixture, meaning that the shear strength of the AC-13C asphalt mixture was lower than that of the AC-20C mixture. However, as the temperature increased, the gap gradually decreased. As the temperature increased from 40°C to 60°C, the deformation strength of the AC-13C asphalt mixture decreased by 56.12%, and that of the AC-20C asphalt mixture decreased by 63.67%. The decrease in the deformation strength of the AC-20C asphalt mixture was greatly affected by the temperature increase. The deformation strength of the AC-13C and AC-20C asphalt mixtures exhibited a linear exponential decrease as the temperature increased. The determination coefficients of the AC-13C and AC-20C mixtures were 0.99858 and 0.99837, respectively.

The deformation strength of the two asphalt mixtures was fitted with the compressive strength, the compressive resilience modulus, and the dynamic stability, respectively, and the obtained parameters are shown in Table 5.

The correlation analysis diagram of the compressive strength and deformation strength of the two asphalt mixtures at different temperatures are presented in Figure 19. Furthermore, Figure 20 shows the correlation analysis diagram of the compressive rebound modulus and the deformation strength of the two asphalt mixtures at different temperatures. The comparison of Figures 19 and 20 reveals a strong linear correlation between the resilience modulus of the asphalt mixture and the deformation strength. The linear correlation coefficients of the two asphalt mixtures were 0.9999 and 0.9969. The linear correlation between the compressive strength and deformation strength was acceptable, and the linear correlation coefficients of the two asphalt mixtures were 0.9292 and 0.9528. It can be concluded that the compressive performance of an asphalt mixture is approximately reflected by its deformation strength.

Figure 21 presents the linear correlation analysis diagram of the deformation strength and dynamic stability of the two asphalt mixtures at different temperatures. The linear correlation coefficients of the AC-13C and AC-20C asphalt mixtures were 0.9756 and 0.9521, respectively. A strong linear correlation between the deformation strength and the dynamic stability of the two asphalt mixtures was observed at different temperatures. The high-temperature shear performance of asphalt mixtures can be reflected by the deformation strength.

4.5. Correlation Analysis of the Dynamic Stability, Deformation Strength, and Stiffness Modulus of the Asphalt Mixtures. Figure 22 shows the correlation analysis diagram of the dynamic stability and stiffness modulus of the two asphalt mixtures at different temperatures. Figure 23 shows the correlation analysis diagram of the deformation strength and stiffness modulus of the two asphalt mixtures at the same temperature. The parameters obtained by fitting the dynamic stability, deformation strength, and stiffness modulus of the two asphalt mixtures are shown in Table 6. A good correlation between the dynamic stability and the stiffness modulus of the asphalt mixture was observed, and the coefficients of determination of the two asphalt mixtures were 0.9824 and 0.9686, respectively. Therefore, the dynamic stability of an asphalt mixture can reflect its creep deformation. The correlation between the deformation strength and the stiffness modulus of the asphalt mixtures was acceptable. The coefficients of determination of the two asphalt

Table 5: Parameters obtained by fitting the deformation strength with the compressive strength, compressive resilient modulus, and dynamic stability.

Model and parameters		$Y = aZ + b$		
		a	b	R^2
Deformation strength (Z) and compressive strength (Y)	AC-13C	0.0850	0.2354	0.9292
	AC-20C	0.0426	0.3529	0.9528
Deformation strength (Z) and compressive resilience modulus (Y)	AC-13C	45.2581	−50.3416	0.9999
	AC-20C	30.0516	20.3958	0.9969
Deformation strength (Z) and dynamic stability (Y)	AC-13C	1045.9359	−1929.4719	0.9756
	AC-20C	703.9401	−43.8097	0.9521

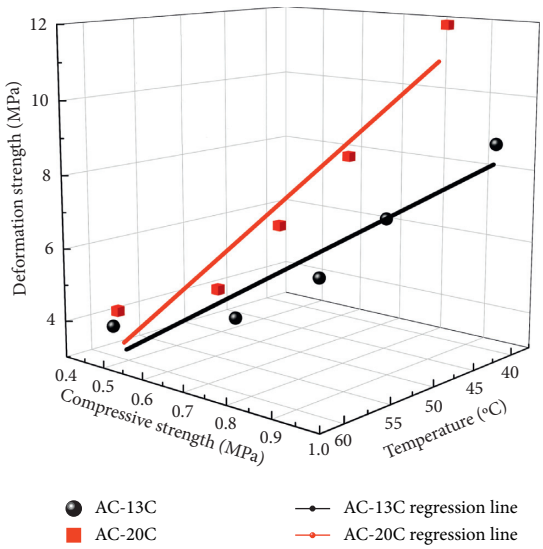

Figure 19: Correlation analysis chart of the deformation strength and compressive strength of the two asphalt mixtures at different temperatures.

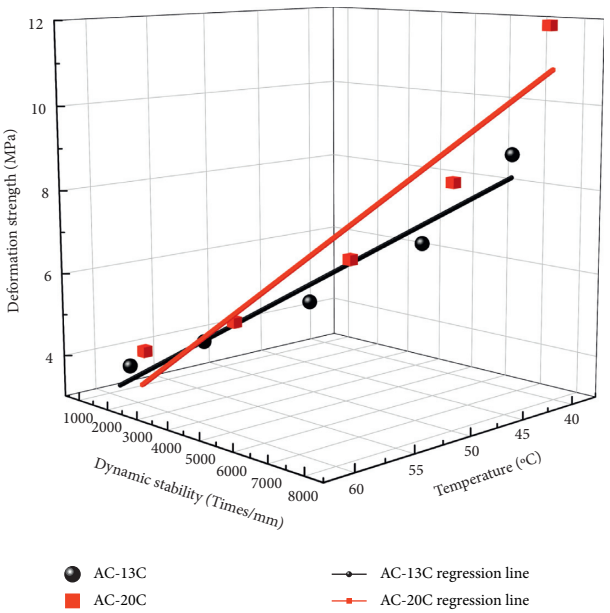

Figure 21: Correlation analysis chart of the deformation strength and dynamic stability of the two asphalt mixtures at different temperatures.

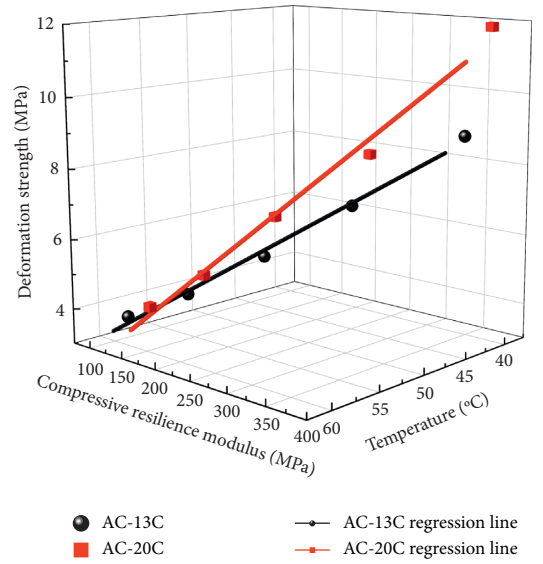

Figure 20: Correlation analysis chart of the deformation strength and compressive resilient modulus of the two asphalt mixtures at different temperatures.

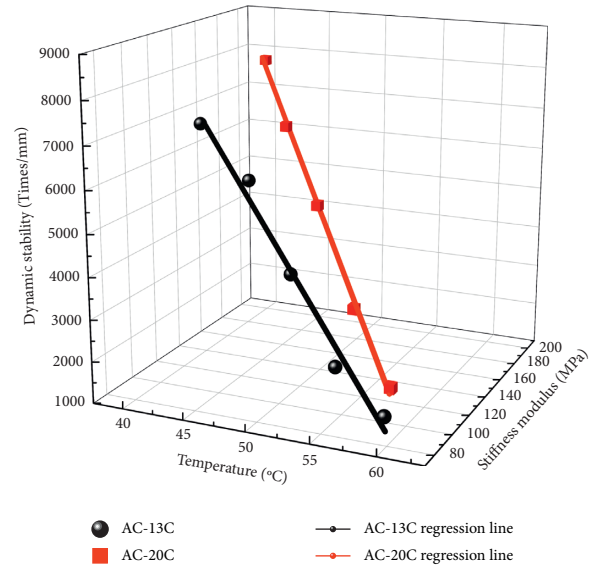

Figure 22: Correlation analysis diagram of the dynamic stability and stiffness modulus of the two asphalts mixtures at the same temperature.

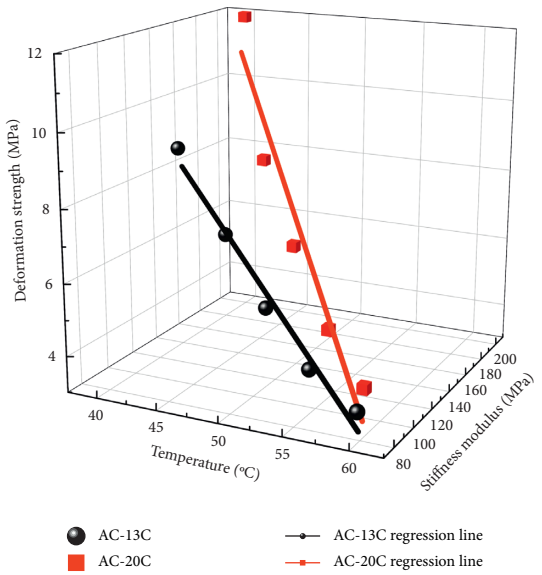

Figure 23: Correlation analysis diagram of the deformation strength and stiffness modulus of the two asphalts mixtures at the same temperature.

Table 6: Parameters obtained by fitting the dynamic stability, deformation strength, and stiffness modulus of the two asphalt mixtures.

Model and parameters		$Z = aY + b$		
		a	b	R^2
Dynamic stability (Z) and stiffness modulus (Y)	AC-13C	48.959	−1838.896	0.9824
	AC-20C	84.392	−5194.909	0.9686
Deformation strength (Z) and stiffness modulus (Y)	AC-13C	0.0753	−2.5306	0.8863
	AC-20C	0.0650	−1.9113	0.9457

mixtures were 0.8863 and 0.9457. Therefore, the deformation strength of an asphalt mixture can approximately reflect its creep deformation.

5. Conclusions

(1) The compressive strength, compressive resilience modulus, and deformation strength of the asphalt mixtures exhibited a linear exponential decrease as the temperature increased. As the temperature increased from 40°C to 60°C, the initial compressive strength of the AC-13C mixture was lower than that of the AC-20C mixture, but the gap between the two gradually narrowed as the temperature continued to increase. The higher the temperature was, the greater the rutting deformation of the asphalt mixture was. The deformation of the AC-13C mixture was larger than that of the AC-20C mixture under the same load and action time. The rutting deformation of the asphalt mixture exhibited a linear exponential increase with the logarithm of time.

(2) The deformation strength showed an excellent correlation with the compressive rebound modulus, compressive strength, and dynamic stability of the asphalt mixtures. Therefore, the deformation strength can be used as an evaluation index of the high-temperature shear performance of the asphalt mixtures.

(3) The deformation strength correlated with the modulus of stiffness of the asphalt mixtures, signifying that the deformation strength can be used as an index to evaluate the high-temperature shear performance of asphalt mixtures.

(4) This article only conducts related research work on the AC-13C and AC-20C asphalt mixtures. More broadly, more research is also needed to determine whether the related properties of other materials and different types of asphalt mixtures are same as those in this article.

Data Availability

The data used to support the findings of this study are included within the article.

Conflicts of Interest

The authors declare that they have no conflicts of interest.

Acknowledgments

This work was supported by the Changjiang Scholars and Innovative Team Development Program of the Ministry of Education (No. IRT1186), the Project of Collaborative Innovation Center of Water Conservancy and Transportation

Infrastructure Safety Protection of Henan Province (No. 2012-6), and the Key Scientific Research Project of Higher Education Institutions of Henan Province (No. 18B580001).

References

[1] K. H. Yati, I. M. Rasdan, K. M. Rehan, K. M. Nuha, and K. M. Suhana, "Evaluation of Permanent deformation of unmodified and rubber-reinforced SMA Asphalt mixtures using dynamic creep test," *Advances in Materials Science & Engineering*, vol. 2015, Article ID 247149, 11 pages, 2015.

[2] J. M. M. Molenaar, H. A. Verburg, and G. E. Westera, "Characterization of permanent deformation behavior of asphalt mixtures," in *Proceedings of the Conference Road Safety in Europ and Strategic Highway Research Program (SHRP)*, Swedish National Road and Transport Research Institute, Prague, September 1995.

[3] I. Hafez, *Development of a Simplified Asphalt Mix Stability Procedure for Use in Superpave Volumetric Mix Design*, University of Maryland, Maryland, 1997.

[4] J. Jiang, F. Ni, L. Gao, and S. Lou, "Developing an optional multiple repeated load test to evaluate permanent deformation of asphalt mixtures based on axle load spectrum," *Construction and Building Materials*, vol. 122, pp. 254–263, 2016.

[5] A. Moriyoshi, N. Takahashi, O. Ikeda, M. Kawashima, and T. Akabane, "Strain distribution in asphalt mixtures during the wheel tracking test at high temperatures," *Construction and Building Materials*, vol. 40, pp. 1128–1135, 2013.

[6] M. Karami, A. Nega, A. Mosadegh, and H. Nikraz, "Evaluation of permanent deformation of BRA modified asphalt paving mixtures based on dynamic creep test analysis," *Advanced Engineering Forum*, vol. 16, pp. 69–81, 2016.

[7] J. Wu, "Uniaxial compression creep prediction of asphalt mixture using the Eshelby equivalent inclusion method," *Advanced Materials Research*, vol. 3683, pp. 410–413, 2015.

[8] B. Fan, X. Yang, and G. Zeng, "Stochastic viscoelastic-viscoplastic response of asphalt mixture under uniaxial compression," *Journal of Engineering Mechanics*, vol. 143, 2017.

[9] S. S. Golsefidi and S. A. Sahaf, "The effect of different loading patterns on the resistance to shear flow of hot mix asphalt," *Construction and Building Materials*, vol. 269, Article ID 121329, 2020.

[10] S. Lijun, *Structural Behavior of Asphalt Pavements*, pp. 501–547, Butterworth-Heinemann, Oxford, United Kingdom, 2016.

[11] Y. Peng, H. Gao, X.-yuan Lu, and Li-jun Sun, "Micromechanical discrete element modeling of asphalt mixture shear fatigue performance," *Journal of Materials in Civil Engineering*, vol. 32, no. 7, 2020.

[12] Y. Zhang, L. Sun, and H. Cheng, "Laboratory performance evaluation of hot-mix asphalt mixtures with different design parameters," *Applied Sciences*, vol. 10, no. 9, 2020.

[13] J. Yuan, J. Lu, and L. Sun, "Evaluation of test method for resistance to permanent deformation of asphalt mixture," *Journal of Chongqing Jianzhu University*, vol. 27, no. 4, pp. 584–609, 2008, in Chinese.

[14] Y. Xu, L. Sun, and L. Liu, "Permanent deformation of asphalt mixture based on uniaxial penetration repeated shear test," *Journal of Tongji University*, vol. 4, no. 8, pp. 1203–1207, 2013, in Chinese.

[15] B. Huang, L. N. Mohammad, and M. Rasoulian, "Three-dimensional numerical simulation of asphalt pavement at Louisiana accelerated loading facility," *Transportation Research Record: Journal of the Transportation Research Board*, vol. 1764, pp. 44–58, 2001.

[16] Y. Cai, "Research on shear strength for asphalt mixture by the uniaxle penetration test method," *Applied Mechanics and Materials*, vol. 97-98, pp. 220–225, 2011.

[17] Ministry of Transport, Prc. Jtg E20–2011, *Standard Test Methods of Bitumen and Bituminous Mixtures for Highway Engineering*, People's Communications Press, Beijing, China, (in Chinese), 2011.

[18] Ministry of Transport, Prc. Jtg E42-2005, *Test Methods of Aggregate for Highway Engineering*, People's Communications Press, Beijing, China, (in Chinese), 2005.

[19] Ministry of Transport, Prc. Jtg F40–2004, *Technical Specifications for Construction of Highway Asphalt Pavements*, People's Communications Press, Beijing, China, 2005, in Chinese.

[20] Y. Doh, K. Yun, S. Amirkhanian, and K. Kim, "Framework for developing a static strength test for measuring deformation resistance of asphalt concrete mixtures," *Construction and Building Materials*, vol. 21, pp. 2047–2058, 2007.